European Polymer Journal 110 (2019) 123–129

Contents lists available at ScienceDirect

European Polymer Journal

journal homepage: www.elsevier.com/locate/europolj

Nondestructive investigation on the nanocomposite ordering upon holography using Mueller matrix ellipsometry

Hao Jiang[a], Haiyan Peng[b,*], Guannan Chen[b], Honggang Gu[a], Xiuguo Chen[a], Yonggui Liao[c,*], Shiyuan Liu[a,*], Xiaolin Xie[c]

[a] State Key Laboratory for Digital Manufacturing Equipment and Technology, Huazhong University of Science and Technology, Wuhan 430074, China
[b] Key Laboratory of Material Chemistry for Energy Conversion and Storage, Ministry of Education, Huazhong University of Science and Technology, Wuhan 430074, China
[c] State Key Laboratory of Materials Processing and Die & Mold Technology, School of Chemistry and Chemical Engineering, Huazhong University of Science and Technology, Wuhan 430074, China

ARTICLE INFO

Keywords:
Nanocomposite
Holography
Diffusion
Photopolymerization
Ellipsometry

ABSTRACT

Ordered materials, which hold organized structures of heterogeneous matter and thus always present superior performance than their non-ordered counterparts, have been constantly pursued. Nevertheless, the direct, precise and nondestructive observation of the ordering process, which is especially critical for evaluating the quality of consecutive manufacturing, remains a formidable challenge. Herein, we introduce Mueller matrix ellipsometry (MME) as a nondestructive method to quantitatively investigate the nanocomposite ordering process upon holography. This nondestructive investigation directly offers the exact width of, refractive index and nanoparticle fraction in each bright (constructive) and dark (destructive) interference area, which is impossible to be implemented using other existing techniques. Interestingly, the width of dark regions in the formed holographic gratings is observed to decrease while the width of bright regions increases with an augmentation of holographic recording time, distinct from previous width-equal assumption. Meanwhile, an apparent diffusion coefficient of $2 \times 10^{-15}\,m^2\,s^{-1}$ for nanoparticles is determined on the basis of time dependent grating parameter variation, which is 3 orders of magnitude lower than the initial value theoretically predicted by the Stokes-Einstein diffusion equation. The distinct diffusion coefficient is attributed to the rapid increase of viscosity driven by polymerization during holography. No depolarization is observed in these holographic polymer nanocomposites, indicating uniform dispersion of nanoparticles in the polymer matrices. The proposed protocol herein is envisioned to pave the way for precisely and nondestructively understanding the formation of ordered structure in electronics, photonics, photovoltaics, biomaterials and other disciplines.

1. Introduction

Ordered materials, which represent organized heterogeneous matter with regulated structures [1], always exhibit superior performance in mechanics, photonics, electrics, bio-functions, and so forth, in comparison with their non-ordered counterparts [1–3]. Holography, with the Nobel Prize fame, is an ideal approach for assembling ordered materials for diverse applications in the fields of 3D image storage, sensors, photonic crystals, and so forth, due to its unique capabilities of simultaneously reconstituting both the amplitude and phase information of coherent lights in materials over a large area [4,5]. Ordering of polymer nanocomposites using holography has attracted special attention not only because of the affordable larger than 5×10^{-3} of refractive index modulation and greatly depressed volume shrinkage [4–8], but also due to the promising high-density data storage in lightweight and flexible devices. In addition, the broad availability of nanoparticles such as gold [9], zirconia [10], titania [11,12], silica [13], zeolite [14], ZnO [15] and ZnS [4,16] enables versatile ordered functional nanocomposites.

Typically, the fundamental principle for the ordering of polymer nanocomposites upon holography is the photopolymerization induced phase separation. Such a process gives rise to predesigned periodical distribution of matter and corresponding refractive index in the recording media. The matter redistribution relies on their diffusion, which is mainly governed by the chemical potential gradient resulting from photopolymerization, and thus is highly dependent on the reaction kinetics and polymerization gelation [4,5]. As depicted in Fig. 1a, photoactive monomers are consumed in the high light-intensity regions

* Corresponding authors.
E-mail addresses: hypeng@hust.edu.cn (H. Peng), ygliao@hust.edu.cn (Y. Liao), shyliu@hust.edu.cn (S. Liu).

https://doi.org/10.1016/j.eurpolymj.2018.11.023
Received 4 August 2018; Received in revised form 28 September 2018; Accepted 14 November 2018
Available online 14 November 2018
0014-3057/

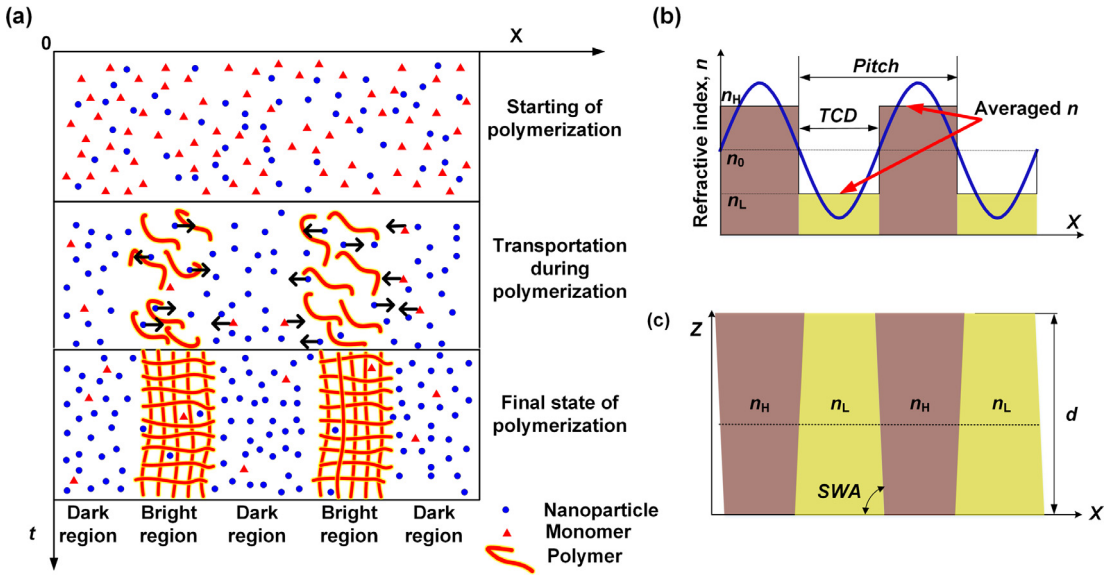

Fig. 1. Process of nanoparticles assembly and refractive index change during holographic photopolymerization. (a) Spatial distribution of nanoparticles, monomers and polymers as a function of time *t* when illuminated by an interference pattern, (b) spatial distribution of refractive indices of a holographic grating at specific time, (c) a general cross section profile of a holographic grating after recording.

during holography because of the light mediated polymerization, leading to the diffusion of monomers towards reactive regions. Subsequently, the photoinert nanoparticles are squeezed into the low light-intensity regions because of the unbalanced chemical potential [17,18]. A sinusoidal distribution of refractive index as shown in Fig. 1b is expected during holographic recording. The parameters such as grating pitch and top critical dimension (*TCD*) are determined by the interference pattern of coherent light illumination. If the refractive indices can be averaged in the high and low intensity regions after recording, a general grating profile as shown in Fig. 1c can be achieved.

Despite that extensive efforts have been made on the patterning control in the past decades, the nanoparticle movement process is still unclear. Most researchers use the diffraction efficiency to analyze the diffusion process [19,20]. However, Goldenberg et al. suggested that the diffraction efficiency was not always a good predictor on nanoparticle sequestration because in some cases other factors than the spatial distribution of nanoparticles would affect the diffraction efficiency of gratings [21]. Braun and co-workers employed transmission electron microscopy (TEM) to clearly demonstrate the eventual nanoparticle localization in holographic gratings and then estimated the diffusion coefficient using the Stokes-Einstein diffusion model [22]. Although Braun's results provided optimized nanoparticle sequestration conditions, the process of nanoparticle transportation is not fully understood. Last but not least, the TEM method is destructive to the sample, which may be not applicable to hydrophilic objects because the specimens for TEM characterization are always required to be microtomed in water. Scanning probe microscopy and scanning electron microscopy (SEM) can be used to characterize the grating structure in real space, but fails to point out the nanoparticle location and refractive index of each region because of limited resolution compared to the tiny nanoparticles in several nanometers. More importantly, the existing techniques are incapable of providing time dependent optical parameters such as refractive index in each bright and dark region. Thus, it is highly awaited to explore a new nondestructive method in nanoscale resolution to illustrate the material ordering during the construction of ordered materials.

In this work, we introduce Mueller matrix ellipsometry (MME) as a nondestructive method to characterize the phase separation process during holographic recording for grating composed of poly(acrylate-co-acrylamide) and 5 nm zinc sulfide (ZnS) nanoparticles. Ellipsometry is an optical metrology technique, which uses polarized light to characterize the thickness of thin films and optical constants of both layered and bulk materials, has been recently applied to monitor the critical dimension (CD) of grating structures [23,24]. Comparing with the conventional ellipsometry that can only acquire two ellipsometric angles, MME can provide all 16 elements of the 4 × 4 Mueller matrix. Consequently, MME exhibits superior sensitivity and accuracy on nanostructure metrology due to the rich information such as anisotropy and depolarization acquired [25,26]. We will show the time-dependent exact width of, refractive index, nanoparticle fraction in each bright (constructive) or dark (destructive) interference area using MME, which is distinct from the diffraction efficiency method that only provide the refractive index modulation (i.e., the refractive index difference between bright and dark regions), and therefore enables the possibility to investigate the nanoparticle diffusion process quantitatively. An apparent diffusion coefficient of $2 \times 10^{-15}\,m^2\,s^{-1}$ is determined on the basis of recording time-dependent variation of grating parameters, which is 3 orders of magnitude lower than the Stokes-Einstein prediction but is more rational because of the rapid increase of viscosity driven by the polymerization during holography.

2. Experimental

2.1. Sample preparation

The synthesis of 5-nm ZnS nanoparticles, the mixtures for holography and their corresponding holographic polymer nanocomposites were prepared according to our previous work [4]. In detail, ZnS nanoparticles were synthesized using one pot reaction of zinc acetate dihydrate, mercaptoethanol, thiourea, and DMF in a three-neck round-bottom flask. The reaction took place at 160 °C with reflux for 12 h under nitrogen gas. Nanoparticles were purified by solvent removal via rotary evaporation at 80 °C and precipitation with 300 mL of ethanol, followed by centrifugation at a speed of 12,000 rpm, and finally washed with methanol for three times. Dry nanoparticles were obtained after room temperature drying under vacuum. Homogeneous holographic mixtures, composed of monomers (N,N-dimethylacrylamide and 6361-100 in a 2:1 wt ratio), 0.6 wt% photoinitibitor (composed of 3,3′-carbonylbis(7-diethylaminocoumarin) and N-phenylglycine in a 1:2 wt ratio), and ZnS nanoparticles with varied loading concentrations, were prepared by ultrasonication at 30 °C for 50 min.

To quantitatively achieve the accurate information in the bright and

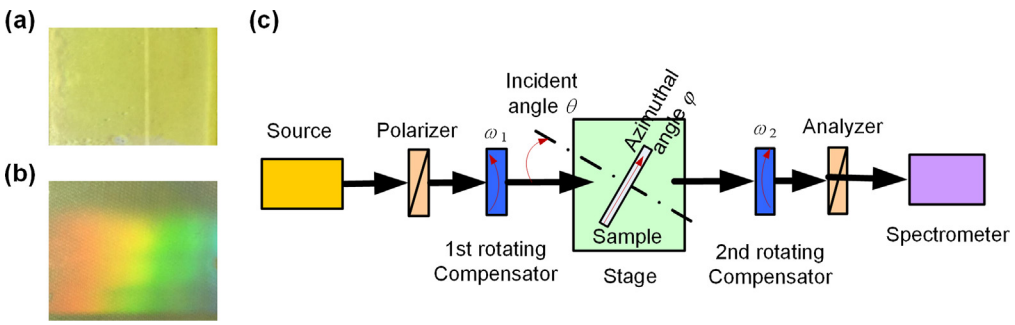

Fig. 2. Typical samples and setups for Mueller matrix ellipsometric characterization. (a) A polymer nanocomposite film with ZnS nanoparticles at a volume fraction of 22.6%, (b) a holographic grating film with an initial ZnS volume fraction of 22.6% (formed by illumination under 5 mW/cm^2 of 442 nm coherent laser patterns for 40 s). (c) Scheme of the dual rotating-compensator MME in the transmission mode.

dark regions of holographic gratings, we prepared a series of nanocomposite films with varied weight fractions of ZnS nanoparticles from 0 to 42 wt% in an interval of 6 wt%, and characterized their bulk refractive indices. These nanocomposite films in thickness of ~10 μm were obtained by exposing the aforementioned homogeneous holographic mixtures under a mercury lamp with a power density of 20 mW/cm^2 for 10 min. The volume fraction of nanoparticles in the nanocomposites was then calculated to be 0–27.3% [4,16]. Fig. 2a shows a typical polymer nanocomposite without holographic recording in which ZnS nanoparticles are uniformly distributed at a volume fraction of 22.6%. By characterizing such a set of nanocomposites, the correlation between the refractive index of the nanocomposites and the loading concentration of ZnS nanoparticles can be established.

Then, the holographic mixtures were added into parallel glass cells with silica spacers in a diameter of ~10 μm. A 442 nm He-Cd laser beam was split into two separate beams with an equal intensity and then simultaneously irradiated the cells to record holographic gratings. Post UV cure was implemented at last to solidify the grating structure with a pitch of 800 nm. The film shown in Fig. 2b represents holographic gratings with an initial ZnS volume fraction of 22.6%. Due to the existence of gratings in the film, rainbow color is clear.

2.2. Instrument configuration

The optical parameters, refractive index n and extinction coefficient k, of the samples with different nanoparticle concentrations, and the optical and profile parameters of the fabricated Bragg gratings were measured using a dual rotating-compensator Mueller matrix ellipsometer (ME-L ellipsometer, Wuhan Eoptics Technology Co., China) [26]. The layout of the MME in order of light propagation was PCr_1SCr_2A, as shown in Fig. 2c, where P and A stood for the polarizer and analyzer, Cr_1 and Cr_2 referred to the 1st and 2nd rotating compensators, and S stood for the sample. With this dual rotating-compensator configuration, the full Mueller matrix elements were obtained in a single measurement. The spectral range of the instrument covers from 200 to 1000 nm. The beam diameter could be changed from the normal value of about 3 mm to a value of less than 200 μm with a focusing lens. Since the possible overlap or partial overlap of the light reflections from the glass surface and the sample might significantly degrade the measurement accuracy in reflection mode, the transmission mode was selected for characterization. In the transmission mode shown in Fig. 2c, the incident angle can be arbitrary selected by rotating the sample stage and the azimuthal angle can be changed by manually rotating the sample.

2.3. Viscosity measurement during photopolymerization

The viscosity measurement of the mixture with an initial ZnS volume fraction of 22.6% was in-situ carried out on a rheometer (Anto-Paar, MCR 302) upon exposure to a monochromatic 442 nm light source with an intensity of 4.5 mW/cm^2 at 30 °C. The mixture was sandwiched between two parallel circular plates in a diameter of 25 mm, in which the bottom transparent acrylic plate enabled the transmission of visible light. The gap between the parallel plates was set as the minimum limit of the instrument, i.e., 0.1 mm.

3. Method

As ellipsometry is a typical model-based metrology, it consists of a forward model followed by an inverse problem solving process. Therefore, appropriate models should be selected for the nanocomposite thin films and gratings.

Since the nanocomposite material in a thickness of 10 μm is transparent in the visible to near infrared range, the optical constant of the studied materials can be characterized by Cauchy model,

$$\begin{cases} n = A + B\frac{1}{\lambda^2} + C\frac{1}{\lambda^4} \\ k = 0 \end{cases} \quad (1)$$

where n represents the measured refractive index, λ is the wavelength, k is the extinction coefficient, A, B and C are constants for the data fitting. In our experiment, in which the incident angle was set to be 60° and the spectral range was 400–1000 nm with an interval of 1 nm.

In grating sample analysis, the rigorous coupled-wave analysis (RCWA) was used to calculate the Mueller matrices [27,28], and the spectral range from 400 to 1000 nm with an increment of 5 nm was selected. The number of retained orders in the truncated Fourier series was 12, and the grating was sliced into 10 layers along the horizontal direction with respect to the grating vector. Therefore, the profile parameters and optical properties to be measured for the grating are: the widths of bright and dark regions, the refractive indices of bright and dark regions, and the side wall angle, which are referred as *TCD*, *TCD'*, n_L, n_H, and *SWA*, respectively. In order to eliminate the effects induced by the variation of sample thickness d, angle of incidence (*AOI*), and angle of azimuth (*AOA*), these three parameters need to be reconstructed in the measurements as well.

The optical constants of the nanocomposite materials and structural parameters of the holographic gratings can be extracted from the measured Mueller matrices, by performing a weighted least-squares regression analysis method (Levenberg-Marquardt algorithm) [29]. This is done by minimizing a weighted mean square error function defined by

$$\chi_r^2 = \frac{1}{15N - P}\sum_{k=1}^{N}\sum_{i,j=1}^{4}\left[\frac{m_{ij,k}^{meas} - m_{ij,k}^{calc}}{\sigma(m_{ij,k})}\right]^2, \quad (2)$$

where k indicates the k-th spectral point from the total number N, indices i and j show all the Mueller matrix elements except m_{11} (normalized to m_{11}), P is the total number of measurands, $m_{ij,k}$ with superscript *meas* and *calc* denote the measured and calculated Mueller matrix elements, respectively, and $\sigma(m_{ij,k})$ is the estimated standard deviation associated with $m_{ij,k}$.

4. Results and discussion

Fig. 3 shows the measured refractive indices of polymer

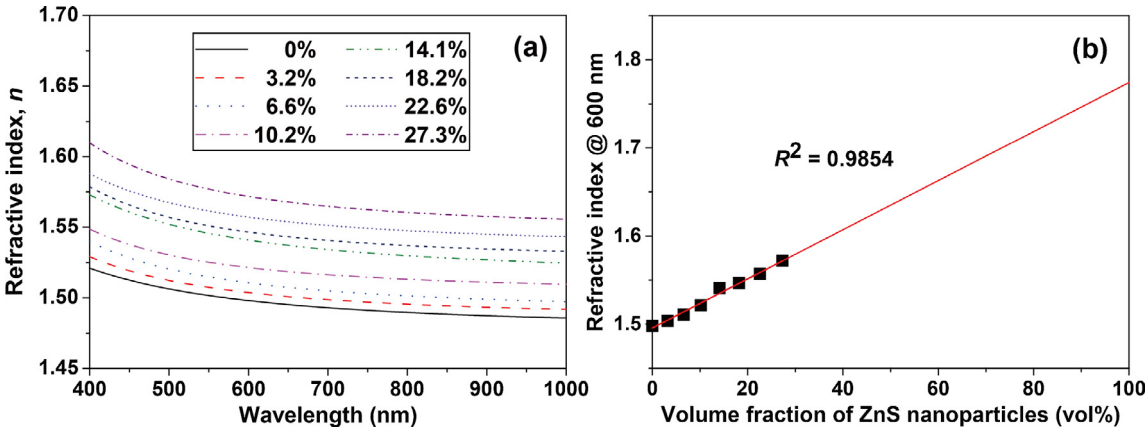

Fig. 3. Correlation of the refractive index of polymer nanocomposites to ZnS nanoparticle concentration. (a) Refractive indices measured by MME when ZnS nanoparticle volume fractions were varied from 0 to 27.3%, (b) refractive index change with respect to ZnS nanoparticle volume fraction at the detection wavelength of 600 nm.

nanocomposites as a function of 5-nm ZnS nanoparticle volume fraction. As shown in Fig. 3a, a consistent increase of refractive index can be observed when the ZnS nanoparticle loading increases. Importantly, a good linear relationship is observed between the refractive index and nanoparticle fractions. A specific example at wavelength of 600 nm is shown in Fig. 3b. The extrapolated n value for the neat ZnS nanoparticles is 1.77, which is in good agreement with the theoretical calculation as described in previous work [4,16]. In other words, the linear relationship between the n value and nanoparticle concentration is expected to be reliable for the polymer nanocomposites in the entire concentration range. These findings benefit us to correlate n value of nanocomposites to nanoparticle concentrations. According to the results shown in Fig. 3b, the refractive index in each region can be converted into the volume fractions of bright and dark regions, as f_1 and f_2, using interpolation. We assume that the pitch of the holographic grating is the same as the interference pattern of illumination light, i.e., 800 nm, and the total fraction of nanoparticle conserves, then the relationship between the widths and fractions can be described by,

$$f_1{*}TCD + f_2{*}(pitch - TCD) = f_0{*}pitch \tag{3}$$

where f_0 is the initial nanoparticle volume fraction. Thus, the parameters need to be directly determined in one measurement are TCD, f_1, d, AOI, AOA and SWA.

Fig. 4 shows an example of the measured and fitted Mueller matrices achieved on one of the grating samples, in which the blue circles represent the measured Mueller matrix elements and the red solid lines represent the calculated ones. The samples stood on the stage with the help of a homemade holder and being initially set as $AOI = 25^\circ$ and $AOA = 25^\circ$. As shown in Fig. 4, the calculated results are in good agreement with the measured values. Additionally, the non-zero elements in off-diagonal blocks such as m_{13}, m_{24}, m_{31}, and m_{42} clearly show the anisotropy of the sample. Since the extinction coefficient of the synthesized ZnS nanocomposites in the measured wavelength region for analysis approximates zero, the absorption of the material is negligible. Thus, we can assume that the detection light can completely penetrate the sample without detectable energy loss, and in the direction perpendicular to the nanocomposite top surface there is no concentration gradient of nanoparticles. Under such conditions, the side wall angle (SWA) shown in Fig. 1c is expected to be 90° and the cross-section profile can be simplified as a rectangle instead of trapezoid. In a preliminary study of holographic grating characterization, the retrieved SWA is 90° with variations within 0.1°, which indicates that our assumption is valid. Therefore, the layer number in RCWA model can be set as 1 and SWA is fixed as a constant angle of 90° in the following experiments to improve the calculation efficiency and the measurement accuracy.

It is worth to mention that, since the initial volume fraction of ZnS nanoparticles reached 27.3%, the agglomeration may exist. If the agglomerate dimension is comparable to the detecting wavelength, scattering effect may become significant and depolarization may arise. Benefit from the advantage of MME, we are able to execute the evaluation of agglomeration for both nanocomposites and holographic gratings based on the depolarization index, DI, defined by [30],

$$DI = \left[\frac{\mathrm{Tr}(\boldsymbol{M}\boldsymbol{M}^{\mathrm{T}}) - m_{11}^2}{3m_{11}^2}\right]^{1/2}, \quad 0 \leqslant DI \leqslant 1, \tag{4}$$

where $\mathbf{M}^{\mathrm{T}}$ is the transpose of Mueller matrix $\mathbf{M}$, while Tr(*) represents the trace. $DI = 0$ and $DI = 1$ correspond to a totally depolarizing and non-depolarizing Mueller matrix, respectively. As shown in Fig. 5, the depolarization index spectra calculated from the measured Mueller matrix spectra of both the nanocomposite and holographic gratings are close to 1 over the entire spectrum range used for analysis, which indicates that no agglomeration exists or the agglomeration in the specific case will not significantly affect the measurement accuracy.

We further performed the analysis on the phase separation process during holographic recording. Fig. 6a–c shows the time-dependent widths, volume fractions of bright and dark regions, and segregation degrees during holography. Benefit from the absolute volume fractions directly measured, the segregation degree, referred as SD, can be calculated as brief as,

$$SD = (f_2 - f_1)/2f_0 \times 100\% \tag{5}$$

where f_2, f_1, and f_0 represent the volume fractions in dark regions, bright regions, and the initial volume fraction, respectively.

In previous reports to date, to calculate the SD an assumption is required to be made that the widths of dark region and bright region are determined by the illumination pattern only, i.e., the width for each region is assumed to be identical if the interference fringes used are equally designed. The results shown in Fig. 6a clearly show that the width of dark region decreases while the width of bright region increases with the increase of holographic recording time. We can also observe an opposite trend of volume fraction change in these two regions as shown in Fig. 6b. These results indicate that the interface of these two regions has a movement towards the center of dark region. Such a movement is rational because the polymerization speed has a decreasing gradient from the center of bright region to dark region and the nanoparticles in the faster polymerization area have a larger possibility to be trapped by the formed macromolecules, as the residual nanoparticles in bright regions of the final state shown in Fig. 1c. Due to such an movement, the detected refractive index modulation n_{H}-n_{L} using MME is speculated to be higher than that calculated using the

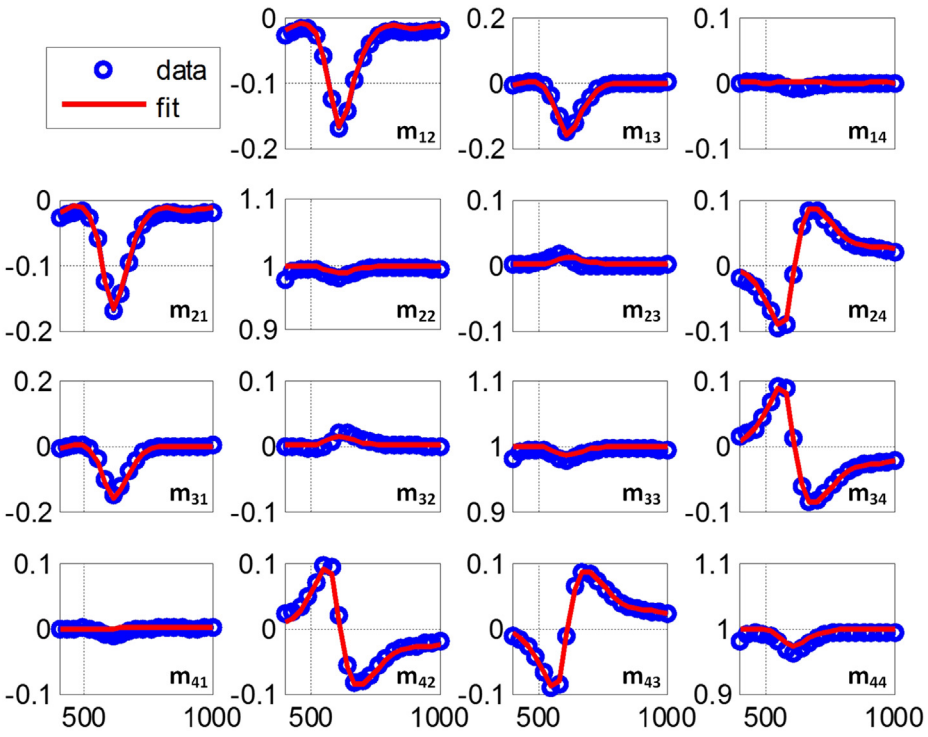

Fig. 4. Calculated and measured Mueller matrix spectra in the transmission mode. The initial ZnS volume fraction was 22.6% and illuminated by the interference light pattern with a period of 800 nm and an intensity of 5 mW/cm^2 for 40 s. The horizontal axes, varying from 400 to 1000 nm with an increment of 5 nm, denote the wavelengths, and the vertical axes denote the values of the associated normalized Mueller matrix elements.

diffraction efficiency method on the basis of Kogelnik's coupled-wave theory [4]. According to our previous disclosures [4,31,32], the time dependent segregation degree, *SD*, can be described as,

$$SD = SD_{\max} \times \left[1 - e^{-\left(\frac{2\pi}{\Lambda}\right)^2 D_a t}\right] \quad (6)$$

where Λ is the grating pitch. The data fit in Fig. 6c with Eq. (6) gives the general time dependent change of *SD* and its maximum value $SD_{\max}$ of 42.2%, which is in good accordance with our previous calculation of 45.3% based on the Kogelnik's coupled-wave theory [4,33]. It is worth to note that the nanoparticles movement is actually driven by both the chemical reactions and their local concentration, whose effects are opposite to each other. Before sufficient gelation, since the nanoparticle concentration is higher in the dark region, backward diffusion driven by the local concentration may exist. Considering the possible backward diffusion after the illumination due to the insufficient gelation, we discard data of *SD* within 10 s for fitting (red points in Fig. 6c). The apparent diffusion coefficient, D_a, achieved from the curve fitting is 2×10^{-15} m^2 s^{-1}. According to the Stokes-Einstein diffusion equation, the diffusion coefficient D of nanoparticles with a radius of r in a solution with a viscosity of η can be described as $D = kT/6\pi\eta r$, where k and T are Boltzmann constant and absolute temperature, respectively. As reported in our previous work, the initial viscosity of the mixture was 26.1 mPa·s before exposure [4]. The fitted diffusion coefficient is 3 orders lower than the initial diffusion coefficient of the 5-nm ZnS nanoparticle (3.4×10^{-12} m^2 s^{-1}) predicted by the Stokes-Einstein diffusion equation.

It is well-known that the viscosity of the mixture increases rapidly during polymerization due to the increasing molecular weight, which gives rise to nanoparticle trapping in growing polymers. Fig. 6d shows the irradiation time dependent viscosity during photopolymerization in a double logarithmic scale. After a short induction period of about 80 s, the viscosity rapidly grows with an exponent of 7.96 ± 0.92 for 35 s and then 17.42 ± 0.76 for another 40 s, i.e. more than 4 orders in magnitude. The hologram sample thickness is ~10 μm, which is only one tenth of that used for the viscosity measurement using photorheology, so the increasing behavior of its viscosity is expected to obey the similar growth scaling but even faster. Therefore, such a slow

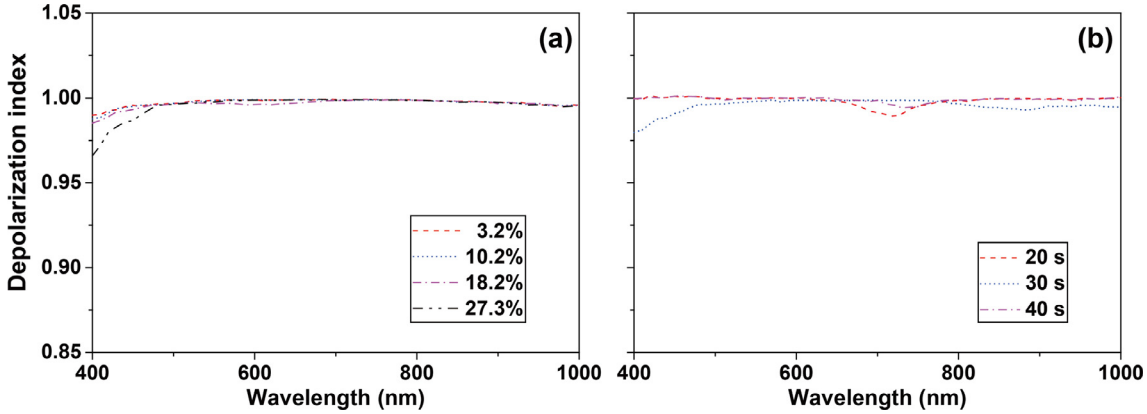

Fig. 5. Depolarization index (a) of nanocomposite with different ZnS volume fractions from 3.2 to 27.3%, (b) of holographic gratings illuminated by the light with an intensity of 5 mW/cm^2 for 20–40 s. The initial ZnS volume fraction was 22.6%.

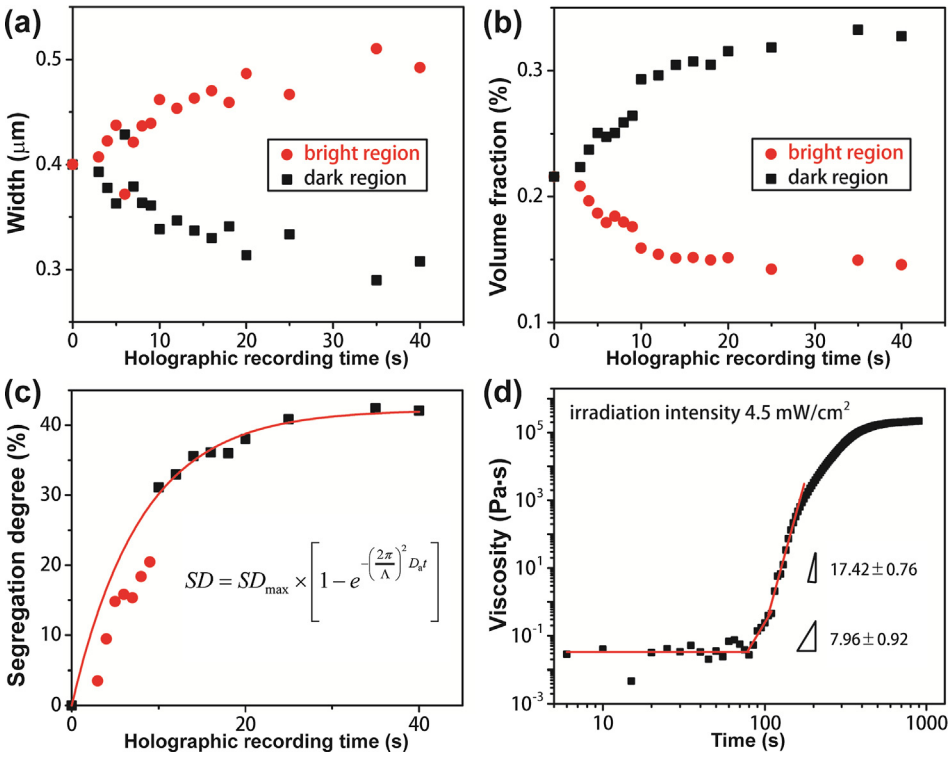

Fig. 6. Time dependent (a) width of dark region (high refractive index and large nanoparticle concentration) and bright region (low refractive index and small nanoparticle concentration), (b) ZnS nanoparticle volume fractions in dark and bright regions, (c) segregation degree during polymerization. (d) Mixture viscosity as a function of irradiation time. The initial ZnS volume fraction was 22.6%, and the irradiation wavelength and intensity were 442 nm and 4.5 mW/cm^2 during the photorheology characterization, respectively.

diffusion process with a coefficient of $2 \times 10^{-15}\,m^2\,s^{-1}$ after 10 s is expected to be rational.

5. Conclusions

In summary, we have introduced MME to characterize the nanoparticle ordering process during holographic recording. Due to the advantages such as fast speed, no destruction, and rich information offered by MME, we measured the time-dependent changes of widths, refractive indices, nanoparticle fractions in bright and dark interference areas during holography, and further analyzed the nanoparticle ordering process during photopolymerization. The observation of decreased dark region width and increased bright region width shows that the polymerization speed gradient should be considered for better understanding the phase separation process instead of using the width-equal assumption. The results also show that the motion of ZnS nanoparticles will be rapidly decreased in the highly viscous media.

Acknowledgments

This work was funded by the National Natural Science Foundation of China (51525502, 51433002, 51575214 and 51503045) and the Natural Science Foundation of Hubei Province of China (2018CFA057).

Data availability

The raw data required to reproduce these findings are available to download from [INSERT PERMANENT WEB LINK(s)]. The processed data required to reproduce these findings are available to download from [INSERT PERMANENT WEB LINK(s)].

References

[1] P. Zavala-Rivera, K. Channon, V. Nguyen, E. Sivaniah, D. Kabra, R.H. Friend, S.K. Nataraj, S.A. Al-Muhtaseb, A. Hexemer, M.E. Calvo, H. Miguez, Collective osmotic shock in ordered materials, Nat. Mater. 11 (2012) 53–57.
[2] P. Heremans, A.K. Tripathi, A.D.J. de Meux, E.C.P. Smits, B. Hou, G. Pourtois, G.H. Gelinck, Mechanical and electronic properties of thin-film transistors on plastic, and their integration in flexible electronic applications, Adv. Mater. 28 (2016) 4266–4282.
[3] J. Wei, Z. Sun, W. Luo, Y. Li, A.A. Elzatahry, A.M. Al-Enizi, Y. Deng, D. Zhao, New insight into the synthesis of large-pore ordered mesoporous materials, J. Am. Chem. Soc. 139 (2017) 1706–1713.
[4] M. Ni, H. Peng, Y. Liao, Z. Yang, Z. Xue, X. Xie, 3D image storage in photopolymer/ZnS nanocomposites tailored by "photoinitibitor", Macromolecules 48 (2015) 2958–2966.
[5] H. Peng, S. Bi, M. Ni, X. Xie, Y. Liao, X. Zhou, Z. Xue, J. Zhu, Y. Wei, C.N. Bowman, Y.-W. Mai, Monochromatic visible light "photoinitibitor": Janus-faced initiation and inhibition for storage of colored 3D images, J. Am. Chem. Soc. 136 (2014) 8855–8858.
[6] R. Ji, S. Fu, X. Zhang, X. Han, S. Liu, X. Wang, Y. Liu, Fluorescent holographic fringes with a surface relief structure based on merocyanine aggregation driven by blue-violet laser, Sci. Rep. 8 (2018) 3818.
[7] L. De Sio, P.F. Lloyd, N.V. Tabiryan, T.J. Bunning, Hidden gratings in holographic liquid crystal polymer-dispersed liquid crystal films, ACS Appl. Mater. Interfaces 10 (2018) 13107–13112.
[8] M. Ni, H. Peng, X. Xie, Structure regulation and performance of holographic polymer dispersed liquid crystals, Acta Polym. Sin. 48 (2017) 1557–1573.
[9] R.A. Vaia, C.L. Dennis, L.V. Natarajan, V.P. Tondiglia, D.W. Tomlin, T.J. Bunning, One-step, micrometer-scale organization of nano- and mesoparticles using holographic photopolymerization: a generic technique, Adv. Mater. 13 (2001) 1570–1574.
[10] G. Garnweitner, L.M. Goldenberg, O.V. Sakhno, M. Antonietti, M. Niederberger, J. Stumpe, Large-scale synthesis of organophilic zirconia nanoparticles and their application in organic-inorganic nanocomposites for efficient volume holography, Small 3 (2007) 1626–1632.
[11] C. Sanchez, M.J. Escuti, C. van Heesch, C.W.M. Bastiaansen, D.J. Broer, J. Loos, R. Nussbaumer, TiO_2 nanoparticle-photopolymer holographic recording, Adv. Funct. Mater. 15 (2005) 1623–1629.
[12] N. Suzuki, Y. Tomita, T. Kojima, Holographic recording in TiO_2 nanoparticle-dispersed methacrylate photopolymer films, Appl. Phys. Lett. 81 (2002) 4121–4123.
[13] T.N. Smirnova, O.V. Sakhno, P.V. Yezhov, L.M. Kokhtych, L.M. Goldenberg, J. Stumpe, Amplified spontaneous emission in polymer-CdSe/ZnS-nanocrystal DFB structures produced by the holographic method, Nanotechnology 20 (2009) 245707.
[14] A.M. Ostrowski, I. Naydenova, V. Toal, Light-induced redistribution of Si-MFI zeolite nanoparticles in acrylamide-based photopolymer holographic gratings, J. Opt. A-Pure Appl. Opt. 11 (2009) 034004.
[15] N. Berberova, D. Daskalova, V. Strijkova, D. Kostadinova, D. Nazarova, L. Nedelchev, E. Stoykova, V. Marinova, C. Chi, S. Lin, Polarization holographic recording in thin films of pure azopolymer and azopolymer based hybrid materials, Opt. Mater. 64 (2017) 212–216.
[16] C. Lü, Y. Cheng, Y. Liu, F. Liu, B. Yang, A facile route to ZnS–polymer nanocomposite optical materials with high nanophase content via γ-ray irradiation initiated bulk polymerization, Adv. Mater. 18 (2006) 1188–1192.
[17] N. Suzuki, Y. Tomita, Real-time phase-shift measurement during formation of a

volume holographic grating in nanoparticle-dispersed photopolymers, Appl. Phys. Lett. 88 (2006) 011105.
[18] Y. Tomita, N. Suzuki, K. Chikama, Holographic manipulation of nanoparticle distribution morphology in nanoparticle-dispersed photopolymers, Opt. Lett. 30 (2005) 839–841.
[19] M. Óscar, M.L. Calvo, J.A. Rodrigo, P. Cheben, F.D. Monte, Diffusion study in tailored gratings recorded in photopolymer glass with high refractive index species, Appl. Phys. Lett. 91 (2007) 141115.
[20] J. Klepp, Y. Tomita, C. Pruner, J. Kohlbrecher, M. Fally, Three-port beam splitter for cold neutrons using holographic nanoparticle-polymer composite diffraction gratings, Appl. Phys. Lett. 101 (2012) 154104.
[21] L.M. Goldenberg, O.V. Sakhno, T.N. Smimova, P. Helliwell, V. Chechik, J. Stumpe, Holographic composites with gold nanoparticles: nanoparticles promote polymer segregation, Chem. Mater. 20 (2008) 4619–4627.
[22] A.T. Juhl, J.D. Busbee, J.J. Koval, L.V. Natarajan, V.P. Tondiglia, R.A. Vaia, T.J. Bunning, P.V. Braun, Holographically directed assembly of polymer nanocomposites, ACS Nano 4 (2010) 5953–5961.
[23] X.H. Niu, N. Jakatdar, J.W. Bao, C.J. Spanos, Specular spectroscopic scatterometry, IEEE Trans. Semicond. Manuf. 14 (2001) 97–111.
[24] H.T. Huang, W. Kong, F.L. Terry, Normal-incidence spectroscopic ellipsometry for critical dimension monitoring, Appl. Phys. Lett. 78 (2001) 3983–3985.
[25] X. Chen, S. Liu, C. Zhang, Depolarization effects from nanoimprinted grating structures as measured by Mueller matrix polarimetry, Appl. Phys. Lett. 103 (2013) 151605.
[26] S. Liu, X. Chen, C. Zhang, Development of a broadband Mueller matrix ellipsometer as a powerful tool for nanostructure metrology, Thin Solid Films 584 (2015) 176–185.
[27] L. Li, Use of Fourier series in the analysis of discontinuous periodic structures, J. Opt. Soc. Am. A 13 (1996) 1870–1876.
[28] S. Liu, Y. Ma, X. Chen, C. Zhang, Estimation of the convergence order of rigorous coupled wave analysis for binary gratings in optical critical dimension metrology, Opt. Eng. 51 (2012) 081504.
[29] W.H. Press, S.A. Teukolsky, W.T. Vetterling, B.P. Flannery, Numerical Recipes: The Art of Scientific Computing, Cambridge University Press, Cambridge, 2007, p. 57.
[30] J.J. Gil, E. Bernabeu, Depolarization and polarization indices of an optical system, Opt. Acta: Int. J. Opt. 33 (1986) 185–189.
[31] H. Peng, G. Chen, M. Ni, Y. Yan, J. Zhuang, V.A.L. Roy, R.K.Y. Li, X. Xie, Classical photopolymerization kinetics, exceptional gelation, and improved diffraction efficiency and driving voltage in scaffolding morphological H-PDLCs afforded using a photoinitibitor, Polym. Chem. 6 (2015) 8259–8269.
[32] G. Chen, M. Ni, H. Peng, F. Huang, Y. Liao, M. Wane, J. Zhu, V.A.L. Roy, X. Xie, Photoinitiation and inhibition under monochromatic green light for storage of colored 3D images in holographic polymer-dispersed liquid crystals, ACS Appl. Mater. Interfaces 9 (2017) 1810–1819.
[33] H. Kogelnik, Coupled wave theory for thick hologram gratings, Bell Syst. Tech. J. 48 (1969) 2909–2947.